Theoretical description of repeated surface-tension auto-oscillations

N. M. Kovalchuk[1] and D. Vollhardt[2,*]
[1]*Institute for Problems of Material Science, 03142 Kiev, Ukraine*
[2]*Max Planck Institute of Colloids and Interfaces, 14424 Potsdam/Golm, Germany*
(Received 25 March 2002; published 14 August 2002)

A mathematical model is proposed to follow the behavior of a system where a droplet of a surfactant with limited solubility on the tip of a capillary under the free liquid surface dissolves in a container with a unity aspect ratio. Numerical simulations show that instability repeatedly arises and fades in the system, resulting in auto-oscillations of the surface tension in agreement with the experimental data. The system evolution during the oscillation is discussed in detail. It is established that the presence of a boundary in the radial direction is a necessary precondition for the appearance of the second and following oscillations.

DOI: 10.1103/PhysRevE.66.026302 PACS number(s): 47.20.Dr, 68.03.−g, 47.20.Ma, 68.35.Fx

INTRODUCTION

Processes taking place in systems far from equilibrium have been attractive for researchers for many decades. When the system contains liquids with a free interface, hydrodynamic instability driven by the Marangoni effect can accompany the processes of mass and energy transfer [1,2]. Most of the theoretical papers devoted to this problem deal with constant gradients of the temperature or concentration imposed perpendicular to the interface or along it. At the same time in a great number of experimental investigations the gradients change with time and are nonuniform in space. That is why the available criteria are sometimes inadequate to predict the appearance and form of the instability. This is just the case with the phenomenon of the auto-oscillation of surface tension considered below.

Auto-oscillations are observed on the free water surface by the dissolution of a surfactant droplet situated at the tip of a capillary under the surface [3,4]. The water is poured into a glass vessel with aspect ratio (the ratio of the radius to the height) of the order of unity. Diethyl phthalate, aliphatic alcohols, or fatty acids have been used to form the droplet. Oscillations begin after a certain induction time during which the surface tension remains constant. They have an asymmetrical shape starting with an abrupt decrease of the surface tension followed by a gradual increase (Fig. 1). The oscillation period depends on the surfactant properties. Oscillations are absent when the immersion depth of the capillary is smaller than a definite critical value depending on the surfactant properties [4].

Talcum powder placed on the surface displays a rapid surface motion directed from the capillary to the vessel wall simultaneously with the decrease of the surface tension. This shows that the surface-tension auto-oscillations can be related to the development of a convective instability. Oscillations are revealed for surfactants having a density larger (diethyl phthalate) and smaller (alcohols, fatty acids) than water. Therefore, the Marangoni effect is responsible for this phenomenon and the buoyancy can play only a subsidiary role.

The concentration gradient near the surface, and consequently the Marangoni number, which is the criterion of system stability, changes over time and depends on the radial coordinate. That is why it is impossible to explain the auto-oscillation mechanism of the surface tension on the basis of known theories, and a special theoretical study is necessary. In addition, the system geometry is vital for the appearance and characteristics of the auto-oscillations and should be taken into consideration.

An understanding of the processes leading to the development of auto-oscillations of the surface tension might be useful for the investigation of processes in other systems that are far from equilibrium. In particular, a similar hydrodynamic evolution may be a component of the mechanism responsible for the oscillations of the electrical potential across liquid membranes investigated by Arai *et al.* [5–7] and by Maeda *et al.* [8]. Normal and tangential concentration gradients of a surfactant appear at the water/oil interface by mass transfer through an oil membrane. Both gradients change over time and along the interface according to the geometry of the measuring cell. Thus, from the hydrodynamic point of view a system with a liquid membrane is quite similar to those considered in this paper. The form of the oscillations is also very similar in both cases.

The hydrodynamic approach developed here can probably be helpful also for a more thorough understanding of the oscillations of the surface tension observed at the water-oil interface by Dupeyrat and Nakache [9] and studied recently

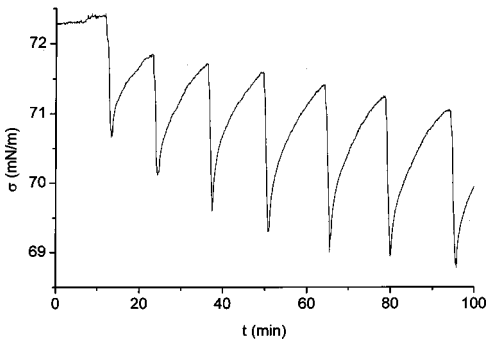

FIG. 1. Auto-oscillations of the surface tension in the system water–diethyl phthalate (experimental results [4]).

*Author to whom correspondence should be addressed.

by Magome and Yoshikava [10].

Numerical simulations of the dynamic behavior of systems with temporally and spatially changing surface concentrations were performed by Jensen and Grotberg [11] and by Matar and Troian [12] for the spreading of an insoluble surfactant over a thin liquid film and by Yeo *et al.* [13] for film drainage between two drops. Because of the system geometry, they used the lubrication approximation where the inertial terms in the Navier-Stokes equations are neglected. On the other hand, these terms are significant for surface-tension auto-oscillation, so in this case the full Navier-Stokes equations should be solved.

Theoretical analysis of the mechanisms leading to the development of auto-oscillations was started in Ref. [3] and proceeded in Refs. [14,15] where a mathematical model was proposed for investigation of the conditions of the instability arising in a semi-infinite liquid layer with a surfactant droplet under the free surface. A direct numerical simulation allowed us to follow the regularities of the model system evolution during the induction period and at the first oscillation. The effect of the surfactant properties on the system behavior at this time was studied as well. But it turned out to be impossible to obtain the second and following oscillations within the limitations of this model. Thus an improved model was needed to clear up the nature of the surface-tension auto-oscillations and the possibility of subsequent oscillations. This paper is devoted to a description of such a model and to discussion of the results of the numerical simulation performed on its basis.

MATHEMATICAL FORMULATION

The model system considered represents a cylindrical vessel filled with an incompressible viscous Newtonian liquid. The upper free surface of the liquid is in contact with a passive gas. A cylindrical capillary is introduced into the liquid. The capillary axis coincides with the vessel axis. A droplet of a surface-active substance having a limited solubility in the liquid is placed on the tip of the capillary. It is assumed that the density of the solution is independent of the concentration and buoyancy can be neglected. The diffusion coefficient of the solute (in the bulk as well as at the surface) and the viscosity of the solution are assumed to be constant. The viscosity of the gas, the intrinsic surface viscosity, the decrease of the droplet volume due to dissolution, and the evaporation of the surfactant from the liquid/gas interface are neglected. The main difference of the model proposed here from that considered in Ref. [14] is the presence of the capillary and the sidewall. The presence of the sidewall is a necessary condition for the appearance of repeated oscillations, as shown below.

The equations governing the behavior of the system are the Navier-Stokes, continuity, and convective diffusion equations. According to the system symmetry it is convenient to use cylindrical coordinates. Experiments with talcum powder show absence of motion in the azimuthal direction. Therefore there is no dependence on the azimuthal coordinate. This gives the possibility of eliminating the pressure by introducing the vorticity and the stream function according to the equations

$$v_r=\frac{1}{r}\frac{\partial\Psi}{\partial z},\quad v_z=-\frac{1}{r}\frac{\partial\Psi}{\partial r},\quad \omega=\frac{\partial v_r}{\partial z}-\frac{\partial v_z}{\partial r}, \tag{1}$$

where r is the radial coordinate, z is the normal to the surface coordinate downward directed with $z=0$ at the surface, v_r and v_z are velocity components in directions radial and normal to the surface, respectively, Ψ is the stream function, and ω is the vorticity.

If time, length, concentration, stream function, vorticity, and velocity are scaled, respectively, by H^2/D, H, c_0, HD, D/H^2, and D/H (here, H is the vessel height, D is the bulk diffusion coefficient of the surfactant, and c_0 is the surfactant solubility) the governing equations in dimensionless form are

$$\frac{\partial\omega}{\partial t}+\frac{\partial(v_r\omega)}{\partial r}+\frac{\partial(v_z\omega)}{\partial z}-\mathrm{Pr}_d\left(\frac{\partial^2\omega}{\partial r^2}+\frac{\partial^2\omega}{\partial z^2}+\frac{1}{r}\frac{\partial\omega}{\partial r}-\frac{\omega}{r^2}\right)=0, \tag{2}$$

$$\frac{\partial^2\Psi}{\partial r^2}+\frac{\partial^2\Psi}{\partial z^2}-\frac{1}{r}\frac{\partial\Psi}{\partial r}-\omega r=0, \tag{3}$$

$$\frac{\partial c}{\partial t}+\frac{\partial(v_r c)}{\partial r}+\frac{\partial(v_z c)}{\partial z}+\frac{v_r c}{r}-\left(\frac{\partial^2 c}{\partial r^2}+\frac{\partial^2 c}{\partial z^2}+\frac{1}{r}\frac{\partial c}{\partial r}\right)=0, \tag{4}$$

where $\mathrm{Pr}_d=\nu/D$ is the diffusion Prandtl number (Schmidt number), ν is the kinematic viscosity of the liquid, and c is the surfactant concentration.

Initially, the liquid is assumed motionless, and the concentration of the surfactant is equal to its solubility on the droplet surface (S) and zero elsewhere, i.e.,

$$\Psi=\omega=v_r=v_z=0,$$

$$c=\begin{cases}1 & \text{if } z,r\in S\\ 0 & \text{elsewhere}\end{cases} \tag{5}$$

at $t=0$. The no-slip condition is used for the wall and the bottom of the vessel, for the capillary and the droplet surface. Then, the dimensionless boundary conditions for the stream function, vorticity, and concentration are

$$\Psi=0,\quad \omega=\frac{1}{R}\frac{\partial^2\Psi}{\partial r^2},\quad \frac{\partial c}{\partial r}=0\quad \text{at } r=R, \tag{6}$$

$$\Psi=0,\quad \omega=\frac{1}{r}\frac{\partial^2\Psi}{\partial z^2},\quad \frac{\partial c}{\partial z}=0\quad \text{at } z=1, \tag{7}$$

$$\Psi=0,\quad \omega=0,\quad \frac{\partial c}{\partial r}=0$$

$$\text{at } r=0\cup h+r_0+\sqrt{r_0^2-r_c^2}<z<1, \tag{8}$$

$$\Psi = 0, \quad \omega = \frac{1}{r}\left(\frac{\partial^2 \Psi}{\partial r^2} + \frac{\partial^2 \Psi}{\partial z^2}\right), \quad c = 1 \quad \text{at } r, z \in S, \quad (9)$$

$$\Psi = 0, \quad \omega = \frac{1}{r_c}\frac{\partial^2 \Psi}{\partial r^2}, \quad \frac{\partial c}{\partial r} = 0$$

$$\text{at } r = r_c \cup 0 < z < h, \quad (10)$$

$$\Psi = 0 \quad \text{at } z = 0, \quad (11)$$

$$\omega = \mathrm{Ma}\frac{1}{(1 - K_L c_0 \Gamma)}\frac{\partial \Gamma}{\partial r} \quad \text{at } z = 0, \quad (12)$$

$$\frac{\partial \Gamma}{\partial t} + \frac{\partial (\Gamma v_r)}{\partial r} + \frac{\Gamma v_r}{r} - \frac{D_s}{D}\left(\frac{\partial^2 \Gamma}{\partial r^2} + \frac{1}{r}\frac{\partial \Gamma}{\partial r}\right)$$

$$- \frac{H}{K_L \Gamma_m}\frac{\partial c}{\partial z} = 0 \quad \text{at} \quad z = 0. \quad (13)$$

Here R is the vessel radius, h is the immersion depth of the capillary, r_0 is the droplet radius, r_c is the capillary radius, Γ is the Gibbs adsorption (scaled by $c_0 K_L \Gamma_m$), K_L and Γ_m are the parameters of the Langmuir isotherm, and $\mathrm{Ma} = RTc_0 K_L \Gamma_m H/\rho \nu D$ is the Marangoni number, R is the gas constant, T is the temperature, ρ is the liquid density, and D_s is the surface diffusion coefficient. Equation (12) is obtained from the tangential stress balance on the free surface by using the Szyszkowsky-Langmuir equation for the surface tension. Equation (13) describes the mass balance on the free surface with the assumption of diffusion controlled adsorption kinetics. It is also assumed that the relationship between the Gibbs adsorption and the adjacent bulk concentration is given by the Langmuir isotherm written for dimensionless variables:

$$\Gamma = \frac{c}{1 + K_L c_0 c}. \quad (14)$$

NUMERICAL SCHEME

A mathematical simulation was performed by using the finite difference method on a regular grid. Equation (3) was solved by the Gauss-Seidel iterative method. For Eqs. (2) and (4) the two-point forward difference approximation is used for the time derivatives, the three-point centered differences are used for the diffusion terms, and the modified upwind differences are used for the convective terms [16]. The use of upwind differences for the convective terms introduces an artificial diffusivity in the numerical scheme. This diffusivity is proportional to the velocity value in the corresponding direction. The analysis of the numerical data shows, however, that the contribution of the convective flux to the concentration change over time is of the same order of magnitude as the contribution of the diffusion flux only when the dimensionless velocity is of the order of 1. The artificial diffusivity is less than 0.01 for this value of the velocity (and for the grid resolution chosen below). It can evidently be neglected in comparison with 1 [the coefficient before the diffusion term in Eq. (4)]. The convective flux is proportional to the velocity and it can be much larger than the diffusion flux at the largest values of the velocity. In this case the contribution of the artificial diffusion coefficient can also be neglected because of the small contribution of the diffusion flux in comparison to the convective flux. The same reasons apply for the vortex transfer.

TABLE I. Calculated induction period depending on the grid resolution.

Grid resolution (mesh point number)	Induction period	
	min	%
20×20	13.1	45.5
40×40	22.6	78.7
80×80	27.4	95.5
120×120	28,7	100

The proper grid resolution was implemented by comparison of the results of the calculations for different grids (Table I). In order to ensure the geometrical similarity of the system used for all the grids considered, the surfactant droplet was modeled as a cylinder of radius $r_0 = 1$ mm and height $h_0 = 2$ mm. The other geometrical parameters were chosen as follows: capillary radius $r_c = 1$ mm, capillary immersion depth $h = 8$ mm, vessel radius $R = 20$ mm, and vessel height $H = 20$ mm. The liquid used was water. The properties of the surfactant (diffusion coefficients $D = D_s = 7.81 \times 10^{-6}$ cm^2/s, solubility in water $c_0 = 5.8 \times 10^{-5}$ mol/cm^3, parameters of the Langmuir isotherm $\Gamma_m = 6.2 \times 10^{-10}$ mol/cm^2, $K_L = 2.3 \times 10^5$ cm^3/mol) are close to those for hexanol and hexanoic acid.

It is seen from Table I that there is a rather large difference between the values of the induction period calculated on grids of 20×20, 40×40, and 80×80 mesh. At the same time the results for the grids of 80×80 and 120×120 mesh differ by less than 5%. Thus the 80×80 mesh provides sufficient accuracy and can be used for the simulation.

RESULTS AND DISCUSSION

Numerical simulation allows us to get the concentration and velocity distributions in the bulk and on the surface at any time and to watch the time evolution of the system. The simulations show that the behavior of the system under consideration depends on the surfactant properties and the system geometry. Examples of the calculated dependencies of the surface tension over time are presented in Figs. 2(a) and 3(a). The simulations were performed for the parameter values given in section ''Numerical scheme'' for a spherical surfactant droplet of radius $r_0 = 1.5$ mm. The immersion depth of the capillary is a geometrical parameter whose influence is particularly strong. Oscillations of the surface tension are absent if the immersion depth is small enough (Fig. 3). Only one oscillation appears at a certain increase in the immersion depth, and finally well shaped regular oscillations are obtained by further increase of the depth (Fig. 2). Thus,

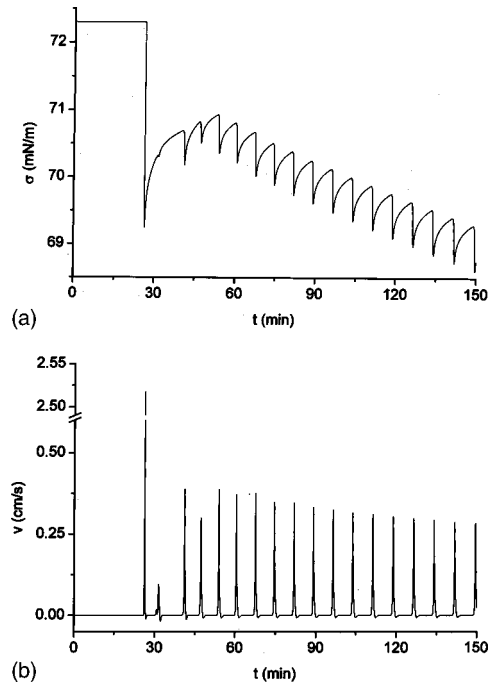

FIG. 2. Results of numerical simulation for the capillary immersion depth $h=8$ mm and the distance from the capillary $r=10$ mm: (a) surface tension vs time; (b) surface velocity vs time.

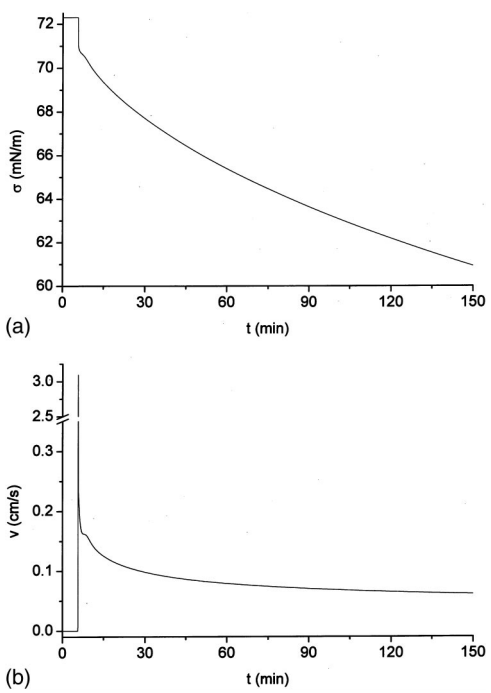

FIG. 3. Results of numerical simulation for the capillary immersion depth $h=4$ mm and the distance from the capillary $r=10$ mm: (a) surface tension vs time; (b) surface velocity vs time.

the model system predicts the same regularities as observed in the experiments [4].

The calculations show the presence of repeated regular oscillation of the surface tension (after several transitional oscillations) for a capillary immersion depth $h=8$ mm [Fig. 2(a)]. Thus, the phenomenon of spontaneous auto-oscillations can be explained within the framework of a simple model, which takes into account only diffusion from the droplet and convection due to the Marangoni effect together with nonuniform adsorption on the free surface. The simulations display, first, that the transition from the slow diffusion regime to a regime with well developed convection is very fast, which looks like an abrupt decrease of the surface tension, and, second, that the transitions between these two regimes can repeat themselves periodically for a long time, as in a real system. The shape of the calculated oscillations is very similar to the shape of the oscillations experimentally observed. Consequently, the proposed model is adequate in describing the mechanism of spontaneous auto-oscillations. Of course, buoyancy, evaporation of the surfactant, mixed (not pure diffusion) adsorption kinetics, surface deformation, and other factors should affect oscillation characteristics such as induction time, period, and amplitude. But the simulations performed demonstrate none of these factors plays a crucial role in the mechanism of auto-oscillations.

The hydrodynamic behavior of the system under consideration resulting in auto-oscillations of the surface tension is evident from the time dependence of the surface velocity presented in Fig. 2(b). The system evolution is characterized by the interchange of two stages. The induction period and the time between the pulses correspond to very slow motion on the surface and in the bulk. At a certain moment the system becomes unstable. The rise of instability reveals itself by a rapid increase of the velocity. The increase of the velocity leads to a considerable acceleration of the mass transfer and simultaneously to the spreading of the surfactant over the interface. This corresponds to a sharp decrease of the surface tension [Fig. 2(a)]. The fast stage continues only for a rather short time. Then the instability fades and the velocity decreases by several orders of magnitude. The system returns to the slow stage. This stage corresponds to a slow increase of the surface tension due to the gradual desorption of the surfactant [Fig. 2(a)]. The nonsymmetrical shape of the auto-oscillation of the surface tension is determined by the differences of the two considered stages. The fast stage is short but is characterized by much more intensive mass transfer than the slow stage.

The velocity change vs time for the capillary immersion depth $h=4$ mm and a distance of 10 mm from the capillary is presented in Fig. 3(b). It is seen that in this case instability also arises. The maximum value of the surface velocity is even larger than for $h=8$ mm [see Fig. 2(b)]. The surface tension sharply decreases after a time of about 6 min caused by the increase of instability [Fig. 3(a)]. However, the further velocity alteration with time, when the instability fades, is very different. After a rather short time the velocity decrease becomes much slower for $h=4$ mm. Later the velocity decreases gradually and remains positive and relatively large over all time. The surface tension also decreases continuously without further oscillations. A completely different dependency was obtained for $h=8$ mm. Here, the velocity decreases rapidly to zero and even becomes negative, i.e., the surface layer of liquid moves to the capillary. The negative

values of the velocity are small and in the course of time the velocity decreases almost to zero. The reverse movement of the liquid always accompanies the repeated oscillations of the surface tension (Fig. 2) and is not observed in the case of a single pulse (Fig. 3). Thus, it might be supposed that the appearance of the liquid motion in the opposite direction is an essential precondition for the repetition of the surface-tension oscillations. We consider now the development of the first oscillation and the conditions for the evolution of the following oscillations in more detail.

The evolution of the system at the initial period, namely, during the induction time and at the beginning of the first oscillation, is not sensitive to the vessel dimensions. It is quite similar to that for the unbounded liquid layer considered in Ref. [14]. During the induction period the surfactant is transferred mainly by means of diffusion. Diffusion forms a spherically symmetrical concentration field in the bulk phase around the droplet. This leads to an inhomogeneous concentration distribution at the gas/liquid interface. The surface concentration has a maximum near the capillary and decreases very fast with increasing distance. For example, the concentration near the wall is 28 orders of magnitude less than that in the vicinity of the capillary in the case presented in Fig. 2 at time $t=26$ min, i.e., at the end of the induction time. The radial distribution of the surface concentration during the development of instability is presented in Fig. 4(a). It is seen that even at the moment of the beginning of instability, the concentration near the wall is some orders of magnitude less than near the capillary (curve 1). The normal concentration gradient near the surface has the same dependency on the radial coordinate. The concentration distribution in the bulk phase is given in Fig. 5. It is nearly spherical at the end of the induction period [Fig. 5(a)].

The surface concentration gradient and the corresponding gradient of the surface tension lead to the appearance of a circular convective motion in the radial direction due to the Marangoni effect. Initially, the center of the convective motion (the point where the stream function has a maximum) is in the vicinity of the capillary. With time the velocity increases according to the increase of the surface concentration and the surface concentration gradient. The location of the stream function maximum moves slowly to the wall. The convective streamlines at the end of the induction period are presented in Fig. 6(a). The velocity distribution near the capillary is also almost insensitive to the vessel dimensions before the beginning of oscillations.

According to the velocity and concentration distribution the convective flux brings a more concentrated solution from the droplet to the surface in the vicinity of the capillary. This leads to a more rapid increase of the normal concentration gradient (Fig. 7) and solute flux to the surface in this region. The surface concentration and the surface concentration gradient increase much faster when convection becomes appreciable. This results in an increase of the surface and bulk velocity which in turn results in a further increase of the normal concentration gradient. Thus, the convection accelerates itself, i.e., instability arises in the system. The development of instability is discussed more comprehensively in Ref. [14].

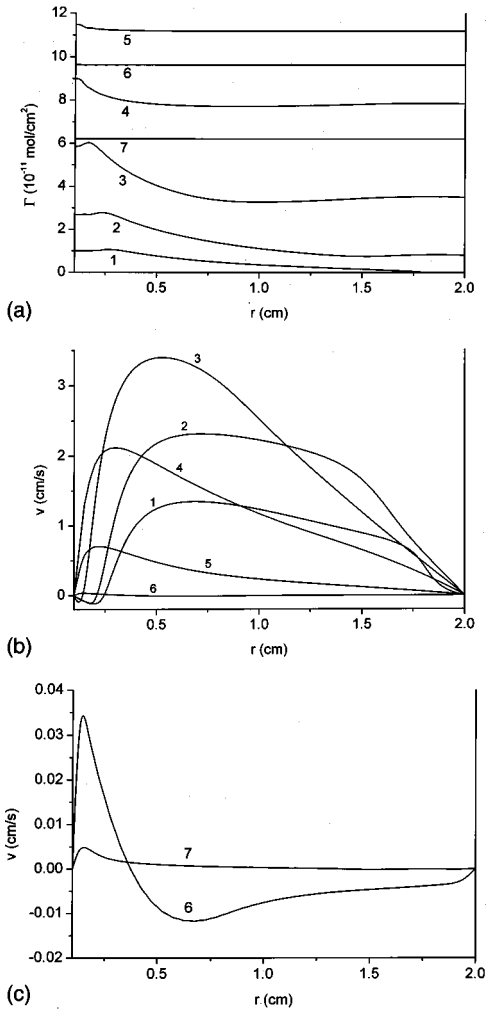

FIG. 4. Radial distribution of surface concentration (a) and surface velocity (b) and (c) for capillary immersion depth $h=8$ mm: curve 1, $t=26$ min 11 s, curve 2, $t=26$ min 12 s, curve 3, $t=26$ min 13 s, curve 4, $t=26$ min 14 s, curve 5, $t=26$ min 20 s, curve 6, $t=27$ min, and curve 7, $t=39$ min 30 s.

Convection spreads the solute over the surface [Figs. 5(b) and 5(c)]. This leads to a sharp decrease of the surface tension over the whole surface. The normal concentration gradient has a maximum near the capillary and decreases very fast with increasing distance (Figs. 7 and 8). The vicinity of the capillary is the region where the solute is supplied to the surface. In the vicinity of the wall the normal concentration gradient near the surface is negative. The solute is supplied in this region due to surface convection. Here, it desorbs and the convective flux removes it [Figs. 5(c) and 5(d)].

It is seen from the radial surface velocity distribution that the velocity decreases sharply near the wall [Fig. 4(b), curves 1 and 2]. This leads to a local surface contraction here and therefore to an increase of the surface concentration near the wall. A reverse surface concentration gradient appears in this region [Fig. 4(a), curves 2–4], which suppresses the surface flow and causes a decrease of the surface velocity [Fig. 4(b), curves 2–4].

Because of the development of instability the maximum of the stream function moves to the wall in the radial direc-

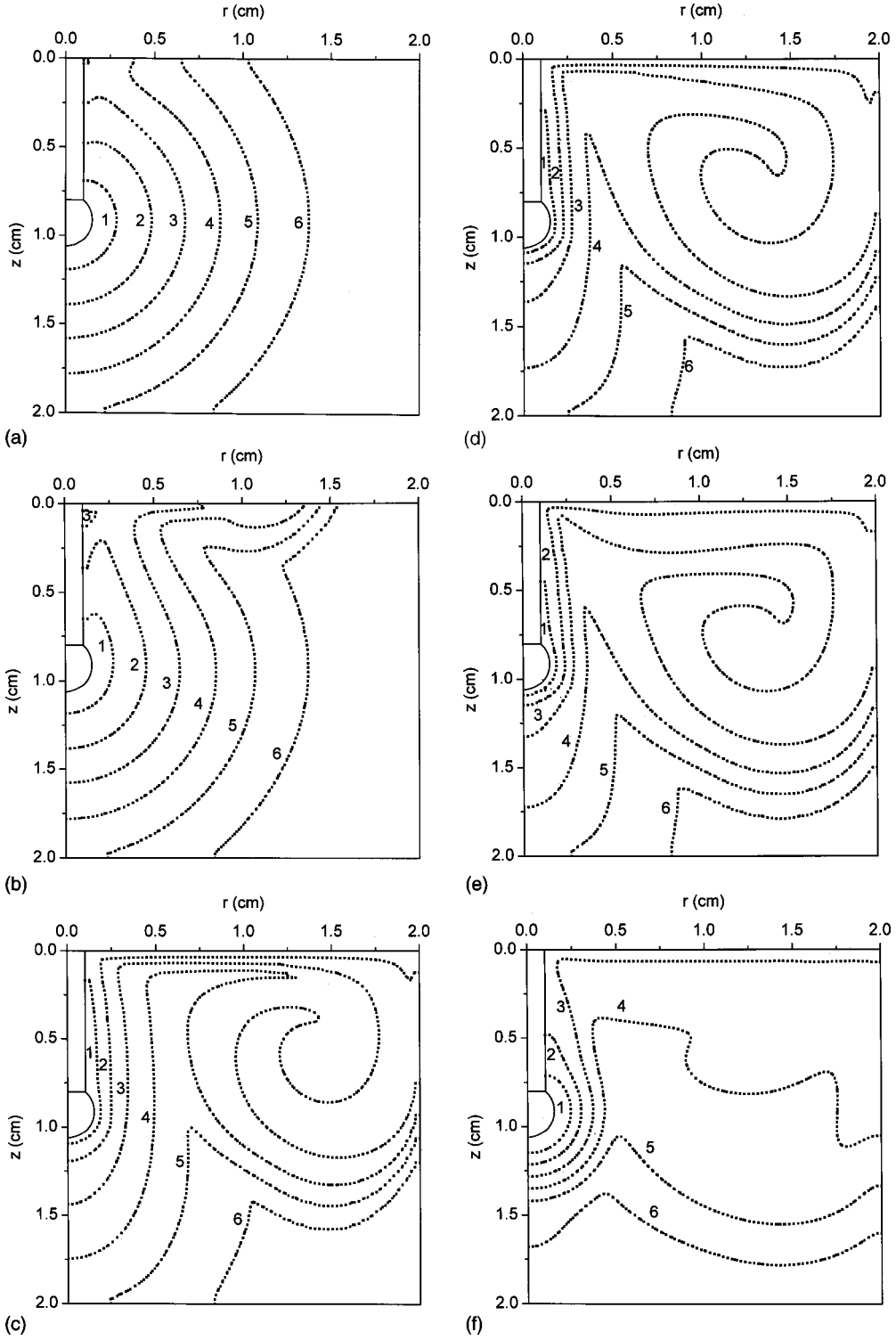

FIG. 5. Concentration distribution in the bulk phase: $t=$(a) 26 min, (b) 26 min 10 s, (c) 26 min 20 s, (d) 26 min 34 s, (e) 27 min, and (f) 39 min 30 s. The values of the dimensionless concentration are as follow: For (a)–(e), curve 1, $c=2\times10^{-1}$, curve 2, $c=10^{-2}$, curve 3, $c=2\times10^{-4}$, curve 4, $c=10^{-6}$, curve 5, $c=10^{-9}$, and curve 6, $c=10^{-14}$. For (f), curve 1, $c=2\times10^{-1}$, curve 2, $c=5\times10^{-2}$, curve 3, $c=8\times10^{-3}$, curve 4, $c=10^{-3}$, curve 5, $c=10^{-4}$, and curve 6, $c=10^{-6}$.

tion and away from the surface in the vertical direction [Figs. 6(b) and 6(c)]. According to the new velocity distribution a more dilute solution is involved in the motion and is supplied to the surface from the bottom [Figs. 5(c)–5(e)]. The normal concentration gradient decreases (Fig. 7) and then decreases the surface concentration near the capillary because of the decrease of surfactant supply and the local surface expansion here [Fig. 4(a), curve 6]. The decrease of the surface concentration and the surface concentration gradient also leads to velocity damping caused by viscous dissipation (along with

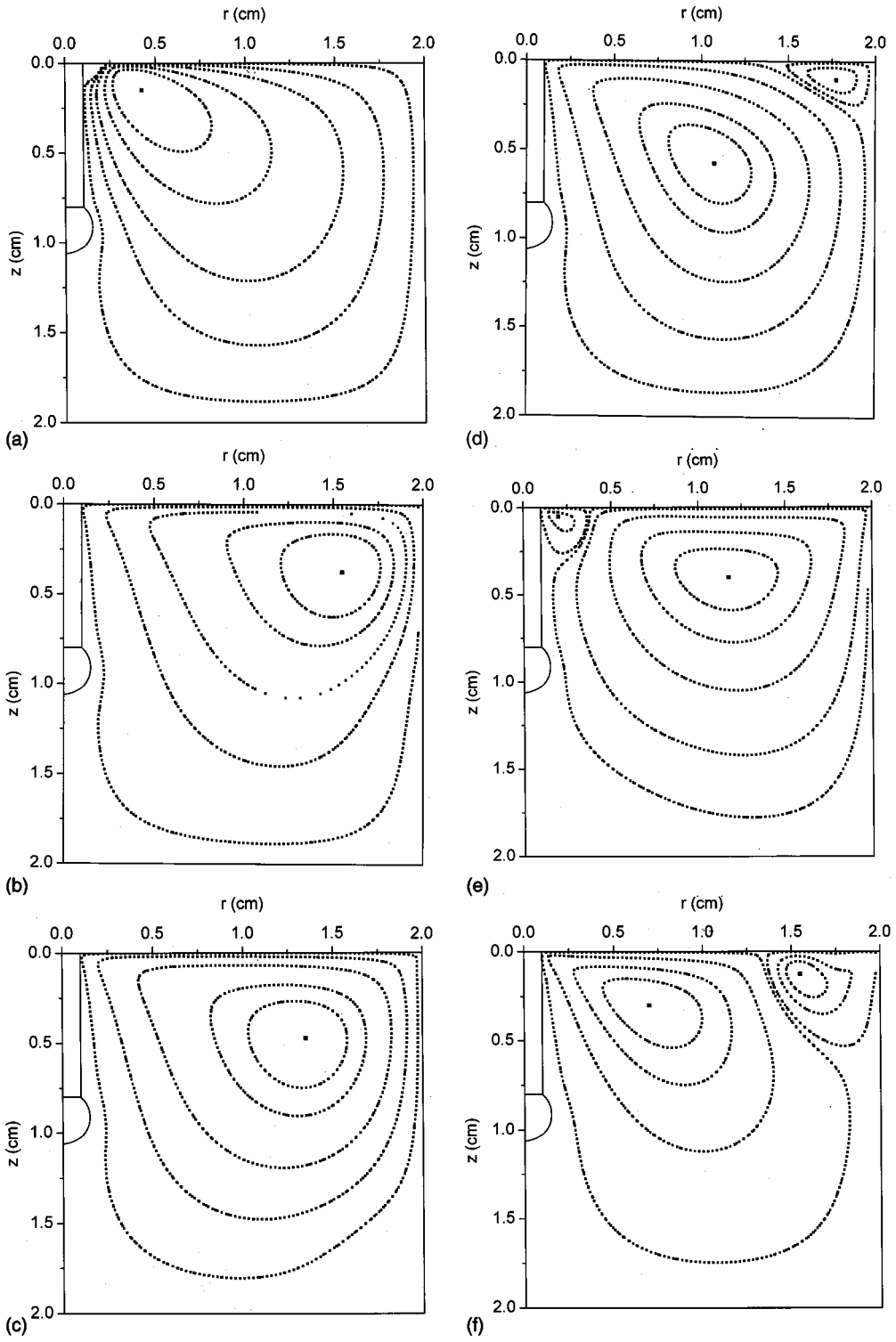

FIG. 6. Streamline distribution in the bulk phase: $t=$(a) 26 min ($\Psi_{max}=27.9$); (b) 26 min 14 s ($\Psi_{max}=15\,904$); (c) 26 min 20 s ($\Psi_{max}=4149$); (d) 26 min 34 s ($\Psi_{max}=731$, $\Psi_{min}=-32.7$); (e) 27 min ($\Psi_{max}=10.7$, $\Psi_{min}=-89.1$); (f) 39 min 30 s ($\Psi_{max}=3.75$, $\Psi_{min}=-0.78$); here Ψ_{max} and Ψ_{min} are the maximum and minimum of the dimensionless stream function, respectively.

the reverse surface concentration gradient near the wall). The instability fades gradually.

The reverse concentration gradient is the reason for the development of the reverse convective roll near the wall [Fig. 6(d)]. This roll expands toward the capillary [Fig. 6(e)]. The velocity on a large part of the surface becomes negative [Figs. 1(b) and 4(b), curve 6, and also the same curve 6 in Fig. 4(c) at higher resolution]. The interaction of the initial and reverse convective rolls causes faster damping of the convective motion due to intensification of the dissipative processes. At this time the convective mass transfer decreases and becomes less than the diffusion mass transfer.

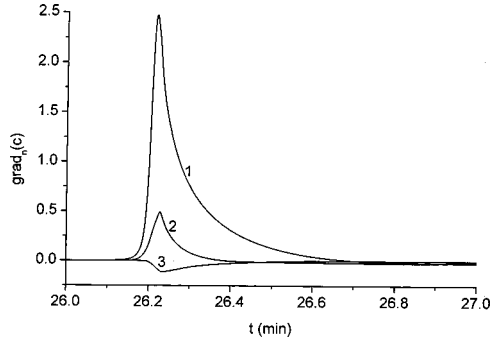

FIG. 7. Dimensionless normal concentration gradient near the surface as a function of time for the distances from the capillary curve 1, $r=1.5$ mm, curve 2, $r=4$ mm, and curve 3, $r=16.5$ mm.

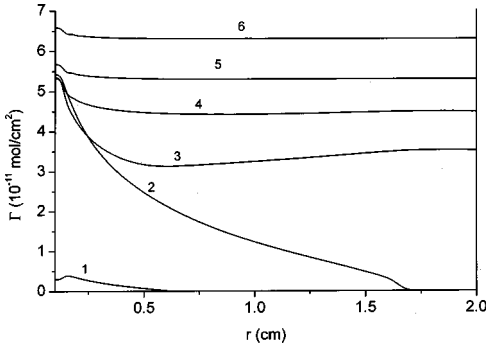

FIG. 9. Radial distributions of the surface concentration for capillary immersion depth $h=4$ mm: curve 1, $t=5$ min 40 s, curve 2, $t=5$ min 41 s, curve 3, $t=5$ min 42 s, curve 4, $t=5$ min 43 s, curve 5, $t=5$ min 50 s, and curve 6, $t=7$ min.

This causes a further decrease of the solute delivery to the surface. The surface concentration becomes almost uniform due to convective and diffusion redistribution of the surfactant [Fig. 4(a), curve 6].

During the slow stage the concentration distribution becomes different over the bulk regions [Fig. 5(f)]. Near the capillary the concentration distribution is nearly spherical or stretched upward. The normal concentration gradient at the surface is downward directed. In more distant surface regions the normal and tangential concentration gradients are lower by some orders of magnitude. The normal concentration gradient is upward directed. The velocity is 3–4 orders of magnitude less than during the fast stage [Fig. 4(c), curve 7]. The reverse roll is reduced [Fig. 6(f)]. The diffusion surfactant transfer is directed to the surface in regions very close to the capillary and from the surface into the bulk in all more distant regions. The general tendency is a slow decrease of the surface concentration at this time.

When the convective mass transfer falls, diffusion from the drop leads to a renewed increase of the concentration in the capillary region close to the surface. Thus the instability develops again after a certain period of time in accordance with the mechanism discussed above, i.e., the next oscillation begins.

It should be noted that the maximum negative value of the surface velocity increases with increase of the mesh point number, which leads to a decrease of the calculated oscillation period. Although the numerical simulations provide lower induction periods (Table I) and higher auto-oscillation periods, the appearance or absence of the reverse liquid motion (from the wall to the capillary) is independent of the grid resolution.

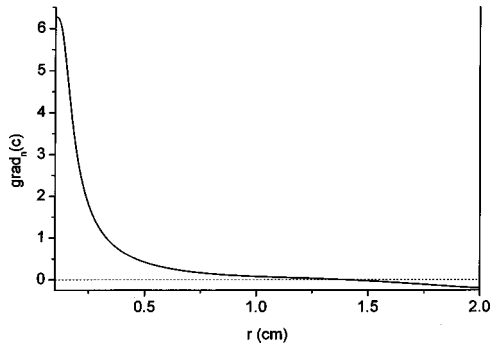

FIG. 8. Radial distribution of the dimensionless normal concentration gradient near the surface at the time $t=26$ min 14 s.

The appearance of the reverse convective roll is the main distinction in the evolution of a system that displays repeated oscillations. It leads to a much faster decrease of convective mass transfer after the oscillation than in the case of a single pulse (oscillation). Development of instability takes place at the capillary immersion depth $h=4$ mm too, resulting in a sharp increase of the surface concentration (Fig. 9, curve 2). The reverse concentration gradient near the surface appears also in this case (Fig. 9, curves 3 and 4). However, this concentration gradient is not sufficient to cause the development of the reverse convective roll. It only shifts the streamlines of the convective motion to the capillary. That is why the velocity decreases much more slowly after the oscillation at $h=4$ mm than after that at $h=8$ mm [cf. Figs. 2(b) and 3(b)]. A small positive tangential concentration gradient exists in the vicinity of the capillary all the time. Surfactant is continuously transferred from the capillary over the whole surface. The surface concentration increases (Fig. 9, curves 5 and 6) and the surface tension decreases gradually without subsequent oscillations [Fig. 3(a)].

As was mentioned above, the solubility and the parameters of the Langmuir isotherm of the surfactant used in the simulations are close to those for hexanol and hexanoic acid. Let us compare the numerical results with the experimental data given in Ref. [17] for the system hexanoic acid–water. This system is chosen because it is less affected by buoyancy than the system hexanol-water, and the presented numerical model does not take buoyancy into account. The experiment reveals an induction time (the time before the first oscillation) of approximately 6 min and oscillation periods in the range of 6–12 min for an immersion depth of the capillary of approximately 9 mm. The calculated induction time is approximately 26 min, and the oscillation period approximately 7 min. The oscillation period increases slightly with time.

The calculated oscillation period agrees rather well with the experimental data. The difference in calculated and experimentally observed induction times may be caused by the

small influence of buoyancy as well as by the peculiarities of the experimental procedure. As a matter of fact the formation of a droplet at the tip of a capillary takes about 2–3 min and is accompanied by motion of the liquid inside the capillary while the injected surfactant passes the capillary. The convective motion accelerates the mass transfer in the vicinity of the surfactant/water interface and creates an initial surfactant distribution near the droplet that causes a decrease of the induction time. This may also be the reason for the difference in the amplitudes of the first and following oscillations [Fig. 2(a)]. The other possible cause of the difference in parameters of the first oscillation may be the neglect of surfactant evaporation in the mathematical model. The evaporation is most intense just during the initial period of time. It is evident, however, that the influence of all the mentioned phenomena requires further investigation.

CONCLUSIONS

Direct numerical simulation demonstrates that the autooscillations of the surface tension on a free liquid surface, caused by dissolution of a surfactant droplet in the bulk phase, can be explained within the framework of a simple model taking into account diffusion, Marangoni convection, and dynamic adsorption. Comparison with experimental data confirms that the model reflects well enough the main regularities of the system behavior. The model is able to describe repeated regular oscillations observed at large capillary immersion depths as well as a single pulse observed at small capillary immersion depths.

The time evolution of the system under consideration is characterized by interchange of slow (diffusion) and fast (convective) stages that determine the oscillating dependency of surface tension vs time. During the induction period, when the surface tension remains nearly constant, as well as during the gradual increase of the surface tension between pulses, convection is weak and diffusion is the main mechanism of surfactant transfer. The sharp decrease of the surface tension corresponds to the onset of instability when the concentration gradient near the surface in the vicinity of the capillary becomes large enough, and convective surfactant transfer becomes predominant in the system. The asymmetrical shape of the oscillation with a sharp decrease and gradual increase of the surface tension corresponds to the different durations of each stage. The fast stage lasts only a short time whereas the slow stage is very prolonged.

The system behavior during the induction period and at the beginning of the first oscillation is independent of the vessel dimensions at any capillary immersion depth. It is close to that for an unbounded liquid layer. In the case of large immersion depth of the capillary, the presence of a boundary in the radial direction is a necessary precondition for the appearance of second and subsequent oscillations (pulses). A reverse concentration gradient arises near the lateral wall due to the local surface contraction. It leads to the development of a reverse convective roll in this region. The interaction of the two convective rolls rotating in opposite directions results in a fast decrease of the velocity due to viscous dissipation, and the system returns to the slow stage when diffusion becomes dominating again. In contrast, if the immersion depth of the capillary is much smaller than the distance to the wall, the influence of the wall is negligible, and the system behaves like an unbounded liquid layer. In this case convection remains dominant all the time after the first oscillation, and subsequent oscillations are not possible. This qualitative difference explains the existence of the critical immersion depth corresponding to the transition from single pulses to repeated oscillations [4].

ACKNOWLEDGMENT

N.M.K. gratefully acknowledges the Max Planck Institute of Colloids and Interfaces for financial support of this work.

[1] *Convective Transport and Instability Phenomena*, edited by J. Zieper and H. Oertel (Braun, Karlsruhe, 1982).
[2] E. L. Koschmieder, *Bénard Cells and Taylor vortices* (Cambridge University Press, Cambridge, England, 1993).
[3] V. I. Kovalchuk, H. Kamusewitz, D. Vollhardt, and N. M. Kovalchuk, Phys. Rev. E **60**, 2029 (1999).
[4] N. M. Kovalchuk and D. Vollhardt, J. Phys. Chem. B **104**, 7987 (2000).
[5] K. Arai, S. Fukuyama, F. Kusu, and K. Takamura, Electrochim. Acta **40**, 2913 (1995).
[6] K. Arai, F. Kusu, and K. Takamura, Anal. Chim. Acta **365**, 279 (1998).
[7] K. Arai and F. Kusu, in *Liquid Interfaces in Chemical, Biological and Pharmaceutical Applications*, Surface Science Series Vol. 95, edited by A. G. Volkov (Dekker, New York, 2001).
[8] K. Maeda, S. Nagami, Y. Yoshida, H. Ohde, S. Kihara, J. Electroanal. Chem. **496**, 124 (2001).
[9] M. Dupeyrat and E. Nakache, Bioelectrochem. Bioenerg. **5**, 134 (1978).
[10] N. Magome and K. Yoshikava, J. Phys. Chem. **100**, 19 102 (1996).
[11] O. E. Jensen and J. B. Grotberg, J. Fluid Mech. **240**, 259 (1992).
[12] O. K. Matar and S. M. Troian, Phys. Fluids **11**, 3232 (1999).
[13] L. Y. Yeo, O. K. Matar, E. S. Perez de Ortiz, and G. F. Hewitt, J. Colloid Interface Sci. **241**, 233 (2001).
[14] N. M. Kovalchuk, V. I. Kovalchuk, and D. Vollhardt, Phys. Rev. E **63**, 031604 (2001).
[15] N. M. Kovalchuk and D. Vollhardt, J. Phys. Chem. B **105**, 4709 (2001).
[16] P. J. Roache, *Computational Fluid Dynamics* (Hermosa, Albuquerque, NM, 1976).
[17] N. M. Kovalchuk and D. Vollhardt, Mater. Sci. Eng. (to be published).